



Synthesis of carbon-13 labelled carbonaceous deposits and their evaluation for potential use as surrogates to better understand the behaviour of the carbon-14-containing deposit present in irradiated PGA graphite

L. Payne ^{a,*}, S. Walker ^b, G. Bond ^b, H. Eccles ^c, P.J. Heard ^a, T.B. Scott ^a, S.J. Williams ^d

^a Interface Analysis Centre, HH Wills Physics Laboratory, University of Bristol, BS8 1TL, UK

^b Centre for Materials Science, University of Central Lancashire, PR1 2HE, UK

^c John Tyndall Institute for Nuclear Research, School of Computing, Engineering and Physical Sciences, University of Central Lancashire, PR1 2HE, UK

^d Radioactive Waste Management, B587, Curie Avenue, Harwell Oxford, Didcot, OX11 0RH, UK

ARTICLE INFO

Article history:

Received 6 April 2015

Received in revised form

15 December 2015

Accepted 18 December 2015

Available online 20 December 2015

ABSTRACT

The present work has used microwave plasma chemical vapour deposition to generate suitable isotopically labelled carbonaceous deposits on the surface of Pile Grade A graphite for use as surrogates for studying the behaviour of the deposits observed on irradiated graphite extracted from UK Magnox reactors. These deposits have been shown elsewhere to contain an enhanced concentration of ¹⁴C compared to the bulk graphite. A combination of Raman spectroscopy, ion beam milling with scanning electron microscopy and secondary ion mass spectrometry were used to determine topography and internal morphology in the formed deposits. Direct comparison was made against deposits found on irradiated graphite samples trepanned from a Magnox reactor core and showed a good similarity in appearance. This work suggests that the microwave plasma chemical vapour deposition technique is of value in producing simulant carbon deposits, being of sufficiently representative morphology for use in non-radioactive surrogate studies of post-disposal behaviour of ¹⁴C-containing deposits on some irradiated Magnox reactor graphite.

© 2015 The Authors. Published by Elsevier B.V. This is an open access article under the CC BY license (<http://creativecommons.org/licenses/by/4.0/>).

1. Introduction

The decommissioning of the UK's first generation of gas-cooled, graphite-moderated (Magnox) reactors will lead to approximately 45,000 m³ of irradiated reactor core graphite, with a packaged volume of 59,000 m³, for geological disposal [1]. An important radionuclide in safety assessments for the disposal of radioactive waste in a geological disposal facility (GDF) is the long lived isotope ¹⁴C (half-life 5730 years) [2]. With an approximate total ¹⁴C activity of more than 7000 TBq arising from Magnox graphite cores and the additional volume of graphite waste arising from advanced gas-cooled reactors (AGR) [2], investigation of the behaviour of ¹⁴C associated with such wastes after closure of a geological disposal facility is important. Whilst reactor graphite has been extensively

studied from a physio-mechanical standpoint, related to core integrity, relatively little research effort has been placed on understanding the behaviour of the graphite and constituent ¹⁴C in a geological disposal environment.

Recent research [3] providing post mortem analysis of irradiated graphite from two Magnox reactor cores highlighted the presence of a carbonaceous deposit on the exposed surfaces of the graphite bricks (channel and interstitial walls) from one of the reactors that has a pronounced and markedly different morphology to the bulk graphite. The extent of this deposit is likely to be a worst case scenario and it is anticipated that not all Magnox reactors may contain such significant deposits. However, these surface deposits have been determined to have a significant ¹⁴C content compared to the bulk graphite [4] that has been created via formation pathways discussed elsewhere [5]. It is not understood how these deposits will behave in a GDF setting in comparison to the graphite which it coats. Specifically there is a gap in the understanding of the release rate and magnitude of the labile ¹⁴C fraction, of which ¹⁴C

* Corresponding author.

E-mail address: liam.payne@bristol.ac.uk (L. Payne).

located in deposited material may contribute significantly, with this labile fraction expected to achieve relatively early release in the lifetime of a GDF [6]. The pronounced “cauliflower-like” morphology observed is not unique to nuclear reactors and similar morphologies have been commonly reported within the scientific literature for carbon from a range of deposition techniques unrelated to nuclear applications [7–11]. At present such deposits are of specific interest in geological disposal of graphite waste from the decommissioning of Magnox reactors, as the deposited material may be present and represent a significant fraction of the labile ^{14}C .

The Magnox reactors represent the first generation of gas-cooled reactors in the UK that used carbon dioxide (CO_2) as the primary coolant and a honeycomb network of graphite bricks to provide neutron moderation. During reactor operation significant amounts of carbon monoxide (CO) was produced from the CO_2 coolant. This CO in turn can be radiolytically polymerised to form a carbonaceous deposit on free surfaces [12]. This non-graphitic carbon deposit is significantly more chemically reactive to air than the underlying graphite [12,13]. During the lifetime of some Magnox reactors, small quantities of methane gas were injected into the coolant gas to inhibit weight loss of the graphite core due to radiolytic oxidation [14]. Methane (CH_4) is a precursor for carbonaceous deposits that form a sacrificial layer protecting the underlying graphite from excessive weight loss [15] and reduction in mechanical strength [16]. It is assumed nitrogen incorporation during deposit formation is the subsequent production route for the high ^{14}C levels observed.

CH_4 is also a commonly utilised feedstock gas for the production of diamond and other carbon coatings by the process of chemical vapour deposition (CVD) [17]. The growth of carbon materials by CVD involves the excitation of a carbon-containing precursor gas using a thermal or plasma energy source that creates activated radicals that will bond to a suitable exposed surface. Therefore, even though differences exist in the formation of carbonaceous deposits from CO and CH_4 , both include the activation of carbon-containing gas creating activated carbon species that will bond to surfaces. Recent work [3] showed that graphite from the Oldbury Magnox power station, which had methane introduced into the coolant gas, had a significant deposit on the fuel and interstitial channel walls of the graphite bricks. This suggested that the deposit formed may be due to methane. A comparison of the morphology and density of such deposits will help determine whether a ^{13}C methane deposit can be used as a simulant for the surface deposit found on irradiated graphite in further work. If ^{13}C carbonaceous deposits can be used as a simulant for the deposits seen on irradiated graphite it will allow easier, non-radioactive investigations of the potential release of ^{14}C from deposits on irradiated graphite in a geological disposal environment including the potential microbial interaction with such material. If the deposits observed on the graphite behave differently to the underlying graphite it may lead to a significantly different release rate for ^{14}C from the deposit than from the underlying graphite when contacted by groundwater some time after the closure of a geological disposal facility. Microbial colonisation may also be more likely on the deposit than the underlying graphite due to the increased surface area due to the amorphous nature of the material.

The use of a ^{13}C simulant allows wider access into the research of nuclear graphite, which contains many other radionuclides such as ^{60}Co , as facilities to handle radioactive materials are not required. Isotopic differences in the precursor material should not alter the chemical nature and/or effect the chemistry of the deposited carbon material. To this end, ^{13}C has previously been used as a common isotopic tracer in biological systems [18] and implanted in graphite [19] as a non-radioactive proxy for ^{14}C . In the current work we demonstrate the use of microwave plasma CVD to create a

carbonaceous layer on graphite substrates that exhibit similar morphologies and densities to deposits observed to have formed in-service on Magnox graphite moderator blocks. The non-radioactive isotope ^{13}C was selected as a tracer during CVD deposition such that deposit–substrate interfaces could be clearly resolved using imaging mass spectrometry analysis to determine the degree of material mixing and substrate etching.

The present work is part of a larger programme (C14-BIG) directed at gaining a better understanding and predicting the release of graphite derived ^{14}C from a GDF and the influence of microbial activity under alkaline conditions expected to predominate for a significant time in a cement-based near field of a geological disposal facility after closure.

2. Experimental

2.1. Sample preparation

Pile Grade A (PGA) graphite was provided by Magnox Limited as a surplus material from the commissioning of the Wylfa nuclear power reactors, Wales. This graphite was trepanned into cores of 12 mm diameter using a stainless steel coring tool. The cores were then cut into 2 mm thick discs using a South Bay Technology Inc. Model 650 low speed diamond cutting wheel with deionised water used as coolant. This process gave a flat surface that was a suitable substrate for deposition. Subsequently ^{12}C and ^{13}C carbonaceous deposits were formed on the graphite surfaces using microwave plasma chemical vapour deposition (MPCVD), Fig. 1.

Coating was carried out using a computer-controlled 2.45 GHz microwave generator (variable power output – maximum 1000 Watts), TE₀₁ single mode cavity (Sairem downstream plasma source WR340), double plunge microwave tuner, mass-flow controllers (MFC) and a carrier (Argon) and precursor gas at a total flow rate of $50\text{ cm}^3\text{ min}^{-1}$. Sample coatings were made at methane concentrations of 2, 10 and 20% for $^{12}\text{CH}_4$ and 2% for $^{13}\text{CH}_4$. For coating, each cylindrical PGA graphite disc was placed on a glass sinter situated inside a quartz tube which was aligned to position the disc within the centre of the waveguide. The tube was then connected to the mass-flow controllers, a gas flow was established and then the system was placed under a low vacuum. Once a 1000 Pa system pressure had been achieved the microwave generator was switched on and the microwave reflectance was reduced, as much as possible, using the double plunge microwave tuner. Once the microwave reflectance was tuned the CVD coating process was left to proceed for a period of 30 min [20].

Additionally, deposition was performed at varying pressures (1000, 5000, 10,000 Pa), however a flow rate of $50\text{ cm}^3\text{ min}^{-1}$ for the gas mixture did not achieve a system pressure of less than 700 Pa. A lower flow rate of $20\text{ cm}^3\text{ min}^{-1}$ was applied at 10% $^{12}\text{CH}_4$ so that a system pressure of 500 Pa could be achieved, additionally growth was performed at 10 Pa system pressure at this reduced flow rate.

1–2 mm particles were also produced alongside the disc samples due to crucible size restrictions for the Linkam catalyst stage for Raman spectroscopy. Additional PGA graphite was provided by the National Nuclear Laboratory (NNL). This graphite was sectioned into smaller rectangular sheets using a JCB toolbox saw and then cut into smaller monoliths using an Erbauer ERB180C tile cutter (with no coolant) thus making the graphite more manageable. The graphite monoliths were then put into a metal container and placed into a 10-ton hydraulic press, where a pressure between 5 and 10 tonnes of pressure was used to break the graphite down into smaller pieces. The pieces were then subsequently filtered using a 3 compartment Fisherbrand stainless steel sieve (aperture sizes: >2 mm, 1–2 mm and <1 mm) and the 1–2 mm particles were

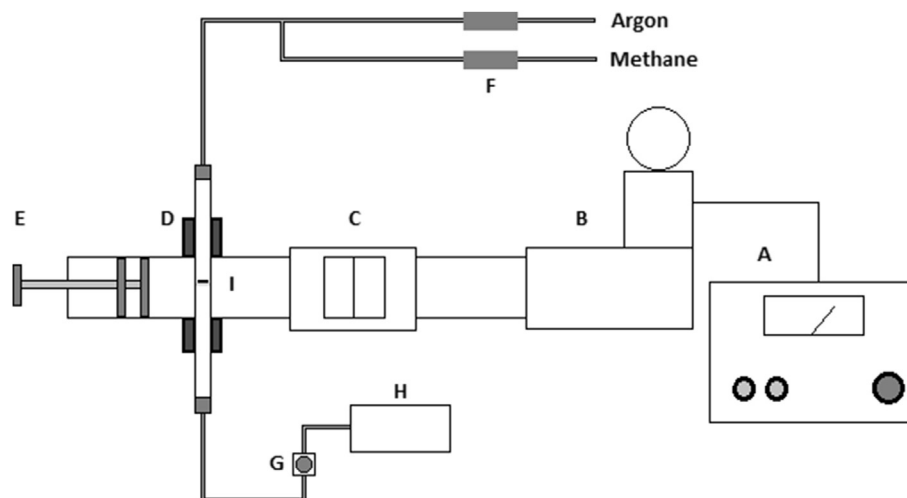


Fig. 1. Schematic diagram of a single mode microwave plasma chemical vapour deposition (MPCVD) system. (A: variable power microwave controller (max. 1000 W); B: air-cooled microwave generator; C: water-cooled circulator; D: 4 port single mode TE01 microwave cavity; E: double plunge microwave tuner; F: mass-flow controllers; G: diaphragm vacuum pump; H: mass spectrometer; I: quartz tube containing a graphite disc on a porous glass sinter.).

retained for subsequent microwave deposition. Both the larger and smaller pieces were repeatedly pressed until all of the graphite was left as a mixture of either particles or powder, following sieving.

A selection of virgin PGA samples (i.e. without deposit) and irradiated graphite specimens extracted by trepanning from a Magnox power station were also analysed for comparison, exact details previously described in Ref. [4].

2.2. Scanning electron microscopy/Focused ion beam

A Helios NanoLab 600i combined SEM/FIB system (FEI, Oregon USA) was used to obtain scanning electron micrographs. The focused ion beam (FIB) was utilised to precision mill trenches to allow the thickness and morphology of the deposit to be determined with nanometre accuracy and to allow subsequent analysis using other techniques.

Electron micrographs were acquired using an accelerating voltage of 15 kV, an electron beam current of 0.17 nA and a dwell time of 100 μ s. Trenches were FIB milled with the use of a Ga^+ ion source with an accelerating voltage of 30 kV. A Selective Carbon Mill (SCM) gas was used throughout to enhance milling rates. The SCM admits small amounts of water vapour directly over the milling area, promoting gasification of the milled material, enhancing the etch rate and reducing redeposition. It also minimises beam damage and therefore reduces the need to deposit platinum on the surface as a protective measure. Initially a 20 nA beam current was used to generate coarsely defined trenches, with subsequent incremental reductions in ion current to reach a final beam current of 0.9 nA for surface finishing. The milled trenches had approximate dimensions of $50 \mu\text{m} \times 56 \mu\text{m} \times 20 \mu\text{m}$ (x, y and z respectively). The trench faces were smooth and flat, allowing for direct and high spatial resolution observation of structures and features.

2.3. Magnetic sector-secondary ion mass spectrometry

For isotopic analysis of the samples, an in-house built magnetic sector secondary ion mass spectrometer (MS-SIMS) was utilised. Full details of the system are described elsewhere [21]. In summary the system comprised of a focused gallium ion gun (FEI electronically variable aperture type) fitted to a Vacuum Generators model 7035 double-focussing magnetic sector mass analyser with a

channeltron detector. The sample was held at a 4 kV potential during analysis. The equipment was controlled using PISCES software, written in-house by Dayta Systems Ltd (Thornbury, UK). The system was capable of providing selected ion mapping and depth profiling with sub-micron resolution.

MS-SIMS analyses were performed in negative ion mode for both spectral acquisition and secondary ion imaging. Mass spectra and depth profiles were initially acquired from 4 different areas of the 2% ^{12}C and ^{13}C methane deposits, detecting mass/charge (m/z) signals at 12, 13, 24 and 26 Da. These ion signals are generated due to the C^- and C_2^- ions derived from sputtered ^{12}C and ^{13}C respectively. Mass spectra were obtained by scanning through the mass range 0–100 Da in 0.05 Da steps, with duration of 100 ms per step and 200 s in total. Data acquisition was performed at a low magnification to reduce beam damage (area analysed $\sim 0.25 \text{ mm}^2$) and with a 3 nA beam current. Identification and calibration of the exact m/z values for use in subsequent depth profiles and images were achieved with the use of these survey spectra.

Depth profiles record the ion yield intensity from selected sputtered analyte ions over time while rastering the ion beam over a selected area. As the deposits are suitably thick it is not anticipated that the depth profile will sputter enough material to immediately expose the underlying graphite. This allows the signal to be averaged over a set period of time and then the ratio between signals to be compared. Depth profiles were acquired for 1800 s with a beam current of 3 nA and area analysed of approximately $2500 \mu\text{m}^2$. Electronic gating was used throughout to eliminate signal created at the margins of the etched area. Signal averages and ratios were calculated from 200 s to 1800 s, disregarding the first 200 s of data as this was the observed transient period for the experiment.

The species compared were the C_2^- ions at 24 and 26 Da, rather than 12 and 13 Da, due to the strong signals obtained from these species, and also to avoid some prominent mass interferences. Interference peaks are difficult to eliminate, however the use of the C_2^- peak is appropriate as the present work is not trying to identify trace elements but aiming to investigate whether the surface deposits are formed of ^{13}C , to what extent ^{13}C is incorporated into the graphite and how thick the overall deposit is.

Secondary ion images were recorded from the FIB milled trenches using the C_2^- ions (24 and 26 Da). The images were obtained by selecting the m/z ratio of the ion of interest, and then

raster scanning the ion beam over a defined area of the sample. The images presented in this paper were acquired over a total area of approximately 0.0225 mm^2 . Each image was acquired over a 60 s period using a 0.3 nA beam current to give the best possible spatial resolution whilst still maintaining sufficient ion signal.

2.4. Catalyst stage Raman spectroscopy

A CCR1000 catalyst stage reactor system connected to a T95 system controller and LinkPad interface (Linkam, Surrey UK) was used for the thermal oxidation of the PGA graphite 1–2 mm particles. For *in situ* spectral acquisition, a LabRAM HR800 confocal Raman microscope (Horiba Jobin Yvon, Kyoto Japan) was used. The sample was heated up in the crucible inside of the catalyst stage from room temperature up to 600°C (at $10^\circ\text{C min}^{-1}$), with a $50 \text{ cm}^3 \text{ min}^{-1}$ flow of air. Spectra were acquired using a 532 nm laser, a 50X long-working distance objective, a 300 g mm^{-1} grating, and spectral acquisition times of 25 s every 50°C .

The heating regime and the spectral acquisition parameters for automated analysis were controlled using a built-in Linkam module script in the Horiba LabSpec 6 software package. The Raman spectroscopy system was calibrated using the 520 cm^{-1} peak from a silicon crystal. Spectral analysis, during thermal oxidation in air, of virgin PGA graphite and PGA graphite with ^{12}C and ^{13}C carbonaceous deposits was carried out to analyse the thermal profile of the surface material (i.e. graphite substrate) and the “cauliflower-like” carbonaceous deposit. This technique allows for analysis of the thermal oxidation properties/reactivity of the different carbon materials and also surface chemical changes due to thermal oxidation.

3. Results

3.1. Scanning electron microscopy

The deposit formed on irradiated graphite taken from Oldbury Magnox reactor has a distinct and pronounced morphology, Fig. 2a, compared to virgin PGA graphite, Fig. 2b [3]. For comparison, electron micrographs of the 2% $^{12}\text{CH}_4$ and 2% $^{13}\text{CH}_4$ deposits can be seen in Fig. 3, a and b respectively. The distinction between deposit and underlying graphite should be noticeable due to the lack of characteristic features in the deposit that are routinely seen in all PGA graphite such as shrinkage cracks and ligaments between pores [22], Fig. 4. The deposits found on irradiated graphite have a ‘cauliflower-like’ appearance due to an agglomeration of irregular spheres, Fig. 5. After FIB milling the internal morphology of the 2% $^{13}\text{CH}_4$ and 2%, 10% and 20% $^{12}\text{CH}_4$ deposited samples can be seen in

Fig. 6a, b, c, and d respectively.

The 2% ^{12}C and ^{13}C methane CVD deposits were observed to have a porous, ‘feathery’ texture that appears to be significantly less dense than the underlying graphite. For the irradiated graphite however, there was very little distinction in density or fine structure between the deposit and the underlying graphite (the deposit appears to have a lower porosity compared to virgin PGA, Fig. 5). It is possible that the underlying PGA graphite in the irradiated samples is protected from radiolytic oxidation by the carbon deposit, leading to the deposit and underlying graphite being difficult to distinguish [15].

Further investigation using greater methane concentrations showed increases in the apparent density of the deposit (which was only determined visually), Fig. 6 (b), (c) and (d), that are more closely comparable to the deposit found on irradiated graphite. Deposits produced at system pressures of 5000 and 10,000 Pa were of different morphology, instead comprising an agglomeration of spherical deposits that were not as extensive or as thick as those grown at the lower pressure of 1000 Pa. Reducing the flow rate to $20 \text{ cm}^3 \text{ min}^{-1}$ allowed a system pressure of 500 Pa to be achieved, however even though the surface topography of the deposit was similar to irradiated material and the other cauliflower-like deposits formed, the internal morphology exhibited extensive porosity and this did not appear suitable as a simulant, Fig. 7(a). Conversely, growth at a system pressure of 1000 Pa at this reduced flow rate formed a deposit that was very similar to that grown at $50 \text{ cm}^3 \text{ min}^{-1}$, Fig. 7(b). The deposit formed at 1000 Pa pressure at 10% methane concentration showed the closest resemblance to those seen on Oldbury irradiated Magnox graphite and was deemed to be the most suitable for use as a simulant.

3.2. Secondary ion mass spectrometry

Survey spectra from the 2% methane ^{12}C and ^{13}C deposits are shown in Fig. 8 (a) and (b) respectively. Signals recorded at mass/charge peaks of 13 Da ($^{13}\text{C}^-$) and 26 Da ($^{13}\text{C}_2^-$) are significantly greater in the ^{13}C deposit compared to the ^{12}C deposit, although these signals are also present in the ^{12}C sample due to $^{12}\text{CH}^-$ and $^{12}\text{CN}^-$ species respectively. The mean ratio ($n = 4$) between the peak heights at 26 Da and 24 Da for the ^{12}C deposit was found to be 0.14 ± 0.03 . The mean ratio ($n = 4$) for the ^{13}C deposit was 115.3 ± 19.1 . This increase of several orders of magnitude is strong evidence that the deposit is predominately ^{13}C as the interfering peak from ^{12}CH at 13 Da is unlikely to be higher in the ^{13}C sample. The errors given here are likely to be due to the strong dependence of signal intensity on location and geometry of the sample in the SIMS system [23].

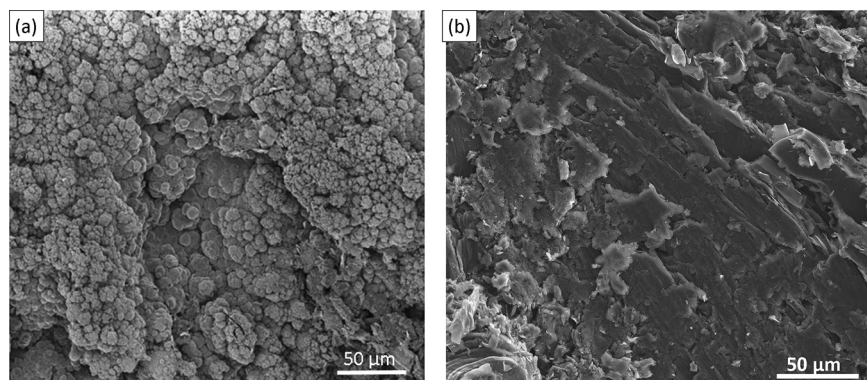


Fig. 2. a) Focused ion beam image of deposit found on irradiated graphite surface, from Ref. [4] and b) virgin PGA surface.

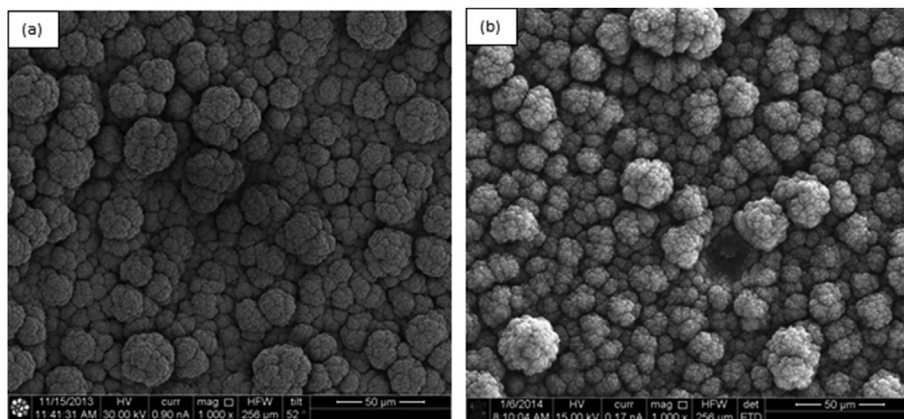


Fig. 3. Scanning electron micrographs from ^{12}C (a) and ^{13}C (b) carbonaceous deposits on Pile Grade A graphite, system pressure 1000 Pa.

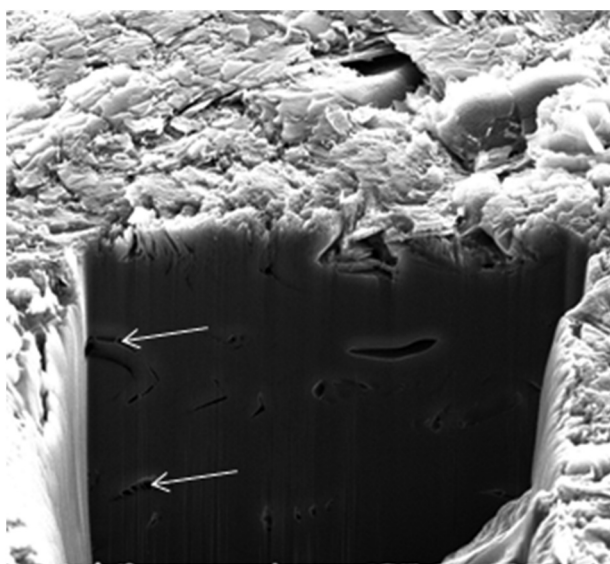


Fig. 4. Scanning electron micrograph from cross section of an uncoated Pile Grade A graphite after FIB milling showing characteristic cracking and ligaments, shown with the arrows.

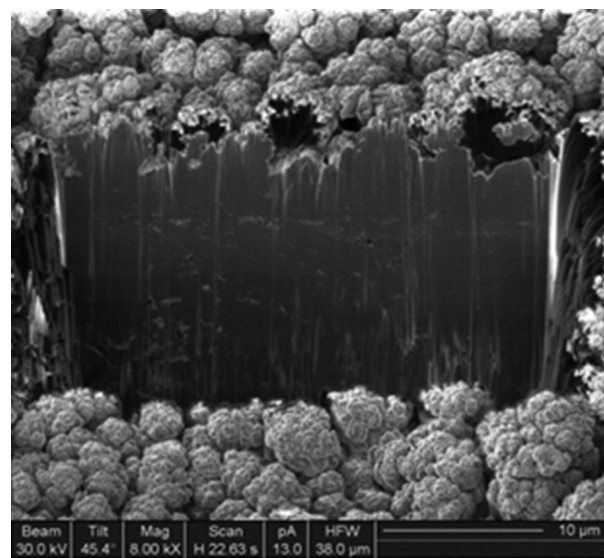


Fig. 5. Focused ion beam image from cross section of channel wall trepanned sample from a Magnox reactor [3].

The areas analysed were selected randomly and the only criteria for examination was that they produced sufficient SIMS signal to allow analysis. Due to the surface not having a uniform, flat surface there are likely to be topographic effects that will affect the signal recorded. This has been studied by other authors [23–25] with suggestions that the changes may be due to the incident angle of the beam, the height of the features and variations in the electric field due to topographic features that may lead to trajectory changes of the secondary ions [24].

SIMS ion signal maps have been recorded for 26 Da and 24 Da for a ^{13}C sample, Fig. 9 (a) and Fig. 9 (b) respectively. For the ^{13}C deposit the mass peak signal at 26 Da is present primarily on the deposit with a significant reduction in signal in the underlying graphite with the 24 Da signal being the reverse, with a more intense signal recorded in the underlying graphite than in the deposit. This shows that the ^{13}C is deposited on top of the underlying graphite. The signal at the bottom of the trench has a relatively high intensity for both 24 and 26 Da, and this may be due to re-deposition of sputtered material originating from the ^{13}C deposit during FIB milling of samples [26].

3.3. Catalyst stage Raman spectroscopy

A three-vectored graph displaying Raman shift, intensity and temperature (x, y and z axis respectively) was used to illustrate the Raman spectra at each temperature during the thermal oxidation experiment. The Raman spectra are displayed between 1100 and 1700 cm^{-1} to allow the critical peaks related to both ^{12}C and ^{13}C carbonaceous materials to be compared. The ^{12}C peaks are the ^{12}D peak at $\sim 1350 \text{ cm}^{-1}$ and the ^{12}G peak at $\sim 1575 \text{ cm}^{-1}$ and the ^{13}C peaks are the ^{13}D peak at $\sim 1300 \text{ cm}^{-1}$ and the ^{13}G peak at $\sim 1525 \text{ cm}^{-1}$.

3.3.1. Virgin PGA

The thermal oxidation spectral profile for a virgin PGA graphite 1–2 mm particle is shown in Fig. 10. This spectral profile shows that there was a negligible change in the intensity of the D and G peaks between 50 and 600 $^{\circ}\text{C}$. This indicates that between 50 and 600 $^{\circ}\text{C}$ the surface of the PGA graphite undergoes very minimal surface oxidation and that the PGA is mostly unreactive.

As the surface of the virgin PGA material remains relatively unchanged during thermal oxidation it will readily allow for any spectral changes, due to the thermal oxidation of ^{12}C and ^{13}C

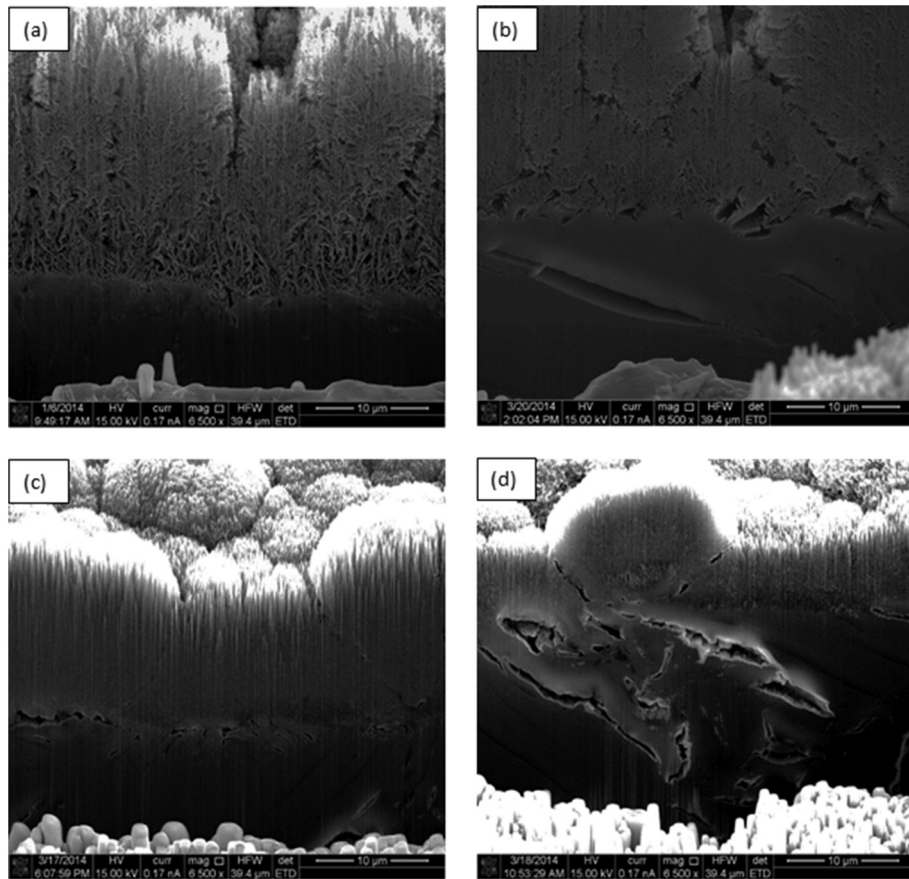


Fig. 6. Scanning electron micrographs showing the ion beam milled cross sections for 2% $^{13}\text{CH}_4$ (a) and 2% (b), 10% (c) and 20% (d) $^{12}\text{CH}_4$ deposited samples, all at system pressure of 1000 Pa.

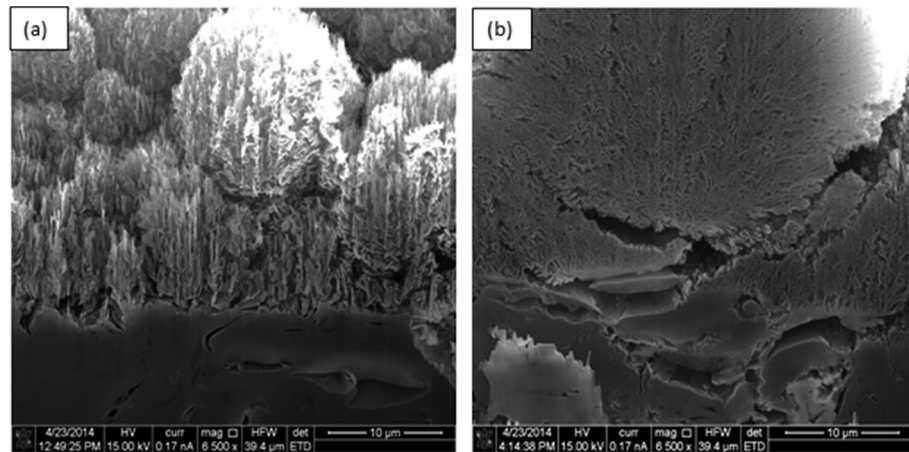


Fig. 7. Scanning electron micrographs showing the ion beam milled cross sections at system pressures of 500 (a) and 1000 (b) Pa, flow rate $20 \text{ cm}^3 \text{ min}^{-1}$.

carbonaceous deposits, to be isolated.

3.3.2. PGA graphite with ^{12}C and ^{13}C deposits

The thermal oxidation spectral profiles for a 2% $^{12}\text{CH}_4$ and $^{13}\text{CH}_4$ deposit on a PGA graphite particle are shown in Figs. 11 and 12 respectively. Fig. 11 shows that there is a noticeable decrease in the ^{12}D peak intensity between 400 and 600 °C. This indicates that the ^{12}C carbonaceous deposit begins to thermally oxidise at approximately 400 °C and appears to have been completely

removed by 600 °C indicated by the intensity of the ^{12}D peak at 600 °C, showing the spectral profile of the virgin PGA graphite material.

There is a noticeable decrease in the ^{13}D & ^{13}G peak intensities between 450 and 600 °C in Fig. 12, which are solely present due to the ^{13}C carbonaceous deposit. This indicates that the ^{13}C carbonaceous deposit begins to thermally oxidise at approximately 450 °C and appears to have been completely removed by 600 °C indicated by the absence of the ^{13}D & ^{13}G peaks at 600 °C, showing the

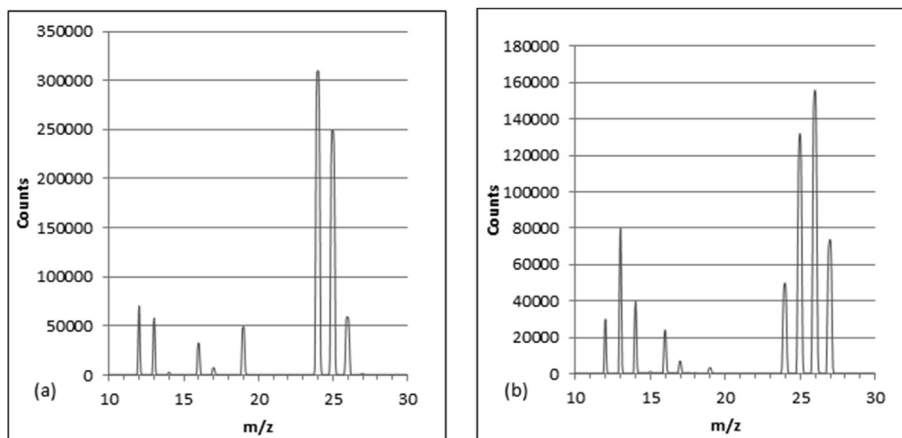


Fig. 8. SIMS spectra from 2% methane ^{12}C (a) and ^{13}C (b) deposit.

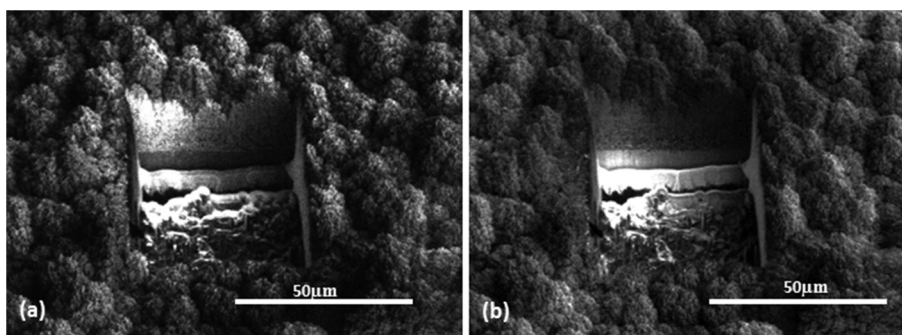


Fig. 9. Secondary Ion signal maps for 26 Da (a) and 24 Da (b) from cross section of ^{13}C carbonaceous deposit on top of Pile Grade A graphite after FIB milling.

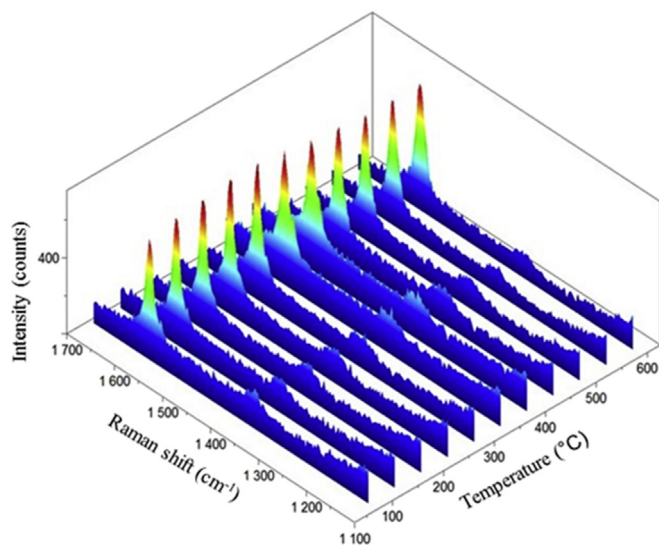


Fig. 10. *In situ* Raman spectral analysis, during thermal oxidation, of a 1–2 mm virgin PGA graphite particle.

spectral profile of the virgin PGA graphite material.

The intensities of the ^{12}D and ^{12}G peaks (PGA graphite) do not decrease but in fact increase relative to the decrease in the intensities of the ^{13}D and ^{13}G peaks (^{13}C carbonaceous deposit), which also illustrates that the surface of the virgin PGA material, as a base substrate, remains relatively unchanged during thermal

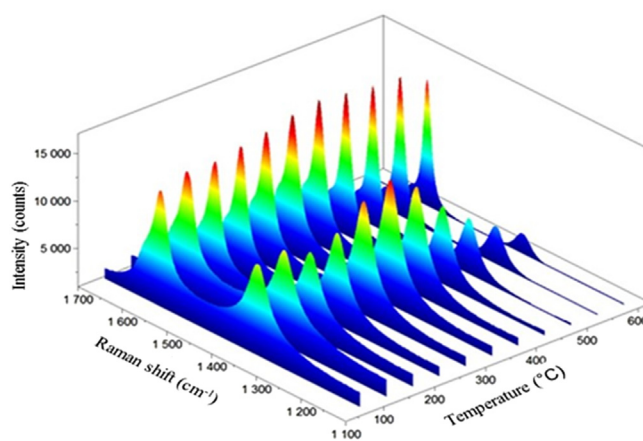


Fig. 11. *In situ* Raman spectral analysis, during thermal oxidation, of a 2% CH_4 ^{12}C carbonaceous deposit on a 1–2 mm PGA graphite particle.

oxidation.

As the Raman peaks associated with the deposits decrease between 400 and 600 °C it indicates that the carbonaceous material on the surface has a similar oxidation temperature to that of the carbonaceous deposits found on irradiated PGA graphite (M. P. Metcalfe, personal communication, 11th November 2013).

Fig. 13 illustrates the isothermal profiles of virgin PGA graphite, irradiated PGA graphite deposit & a ^{12}C microwave simulant deposit at 450 °C, in air, over a 50 h period. The oxidation of virgin PGA

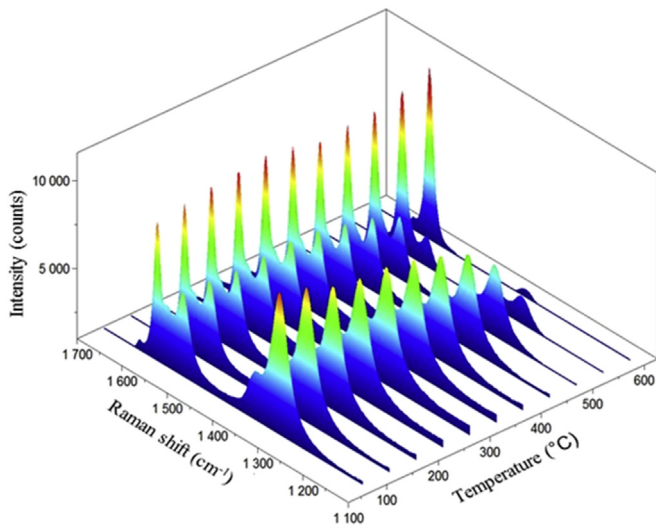


Fig. 12. *In situ* Raman spectral analysis, during thermal oxidation, of a 2% CH₄ ¹³C carbonaceous deposit on a 1–2 mm PGA graphite particle.

graphite is negligible whereas the irradiated PGA graphite deposit & the C-12 microwave simulant deposit show significantly greater rates of oxidation and are clearly more reactive. Initially the rates of thermal oxidation remain fairly similar for the first 5 h for the irradiated PGA graphite deposit & the ¹²C microwave simulant deposit but for the next 45 h the irradiated PGA graphite deposit shows a greater rate of thermal oxidation. This deviation in rates of reactivity may be due to irradiated damage caused to the underlying PGA graphite in the irradiated PGA graphite sample whereas the underlying PGA graphite in the microwave simulant underwent no irradiation and started off as pristine virgin PGA graphite. However the microwave simulant carbonaceous deposit reactivity seen in the TGA isothermal data shows a similar reactivity to that of the carbonaceous deposit seen in irradiated PGA graphite.

4. Discussion

Previous examination [3] of irradiated graphite from Magnox

reactors has shown that during generation lifetime a carbonaceous deposit can be formed on the fuel and interstitial channel walls of the graphite moderator that has a markedly different morphology to the underlying PGA graphite. This work aimed to form a similar carbonaceous deposit using ¹³C precursor gas to allow subsequent investigation of the behaviour of such deposits in leaching and microbial studies pertinent to examining graphite degradation and ¹⁴C release in a GDF [27]. Use of a simulant allows future experiments to be performed more easily than using irradiated graphite due to a removal of the need to work with radioactive materials. However, the use of simulants necessitates care to ensure that they are representative of the properties being examined. With the use of several experimental techniques (FIB, SEM, MS-SIMS, Raman) this work has examined the internal morphology as well as the surface topography of carbonaceous deposits formed using microwave plasma CVD and compared them to irradiated graphite trepanned from a Magnox power station graphite core.

Microwave plasma CVD has been used to form adherent carbonaceous deposits on the surfaces of virgin (unirradiated) PGA graphite discs. Microwave plasma CVD is widely used to grow other carbon materials with differences in growth parameters (precursor gas, temperature, pressure, microwave power) leading to different allotropes being formed most notably Carbon-Nanotubes (CNT) [28,29] and diamond [30,31]. Initially, ¹²C precursor gas, using a system pressure of 1000 Pa with a flow rate of 50 cm³ min⁻¹, was used, primarily due to the high cost of labelled isotopic gases, and with the use of scanning electron microscopy the surface topography was found to be very similar to the 'cauliflower-like' deposits found on irradiated graphite [3]. However, after sectioning with a focused ion beam it was found that the internal morphology was more porous than the deposit found on irradiated graphite. This is believed to be due to the growth rate, approximately 50 μm h⁻¹, of the deposit being too rapid to allow a dense deposit to be formed. By comparison, growth rates of diamond using microwave plasma CVD are usually in the region of 1 μm h⁻¹ [32] and these form 'solid' deposits. By increasing the methane concentration in the precursor gas mix an increased density in the deposit was achieved, likely due to the increased availability of carbon radicals available for deposition. It should be noted that the deposits formed on irradiated graphite are formed at conditions that are very difficult to replicate, pressures of 1–3 MPa, temperatures of approximately 400 °C and in the presence of a neutron flux [33], therefore the high density of the

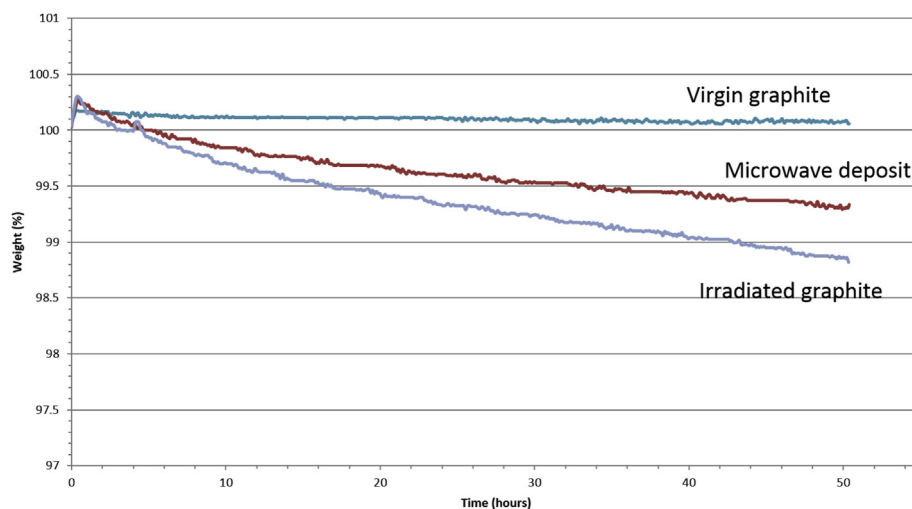


Fig. 13. Thermograms from virgin PGA graphite, irradiated PGA graphite and ¹²C simulant deposit on PGA graphite examined at 450 °C, in air, over a 50 h period.

deposits found on irradiated graphite is likely due to the high pressure environment, whereas in microwave plasma CVD low pressures are used so that the plasma can be sustained.

Further experiments were carried out to investigate the parameters which can affect the growth rate of carbonaceous deposits and to determine whether a more representative carbonaceous deposit could be formed using microwave plasma CVD. Experiments carried out at 200 W using 2, 10 & 20% CH₄ failed to generate carbonaceous deposits. However, deposition at 400 W induced a rapid growth of carbonaceous material.

Further tests were carried out at both 5000 & 10,000 Pa pressures using 10% CH₄. Deposits were produced for both pressures; however these deposits showed a thin agglomeration of carbonaceous spheres on the graphite substrate. This difference in form and thickness shows that growth at higher pressures is not suitable in producing an analogous material for studying irradiated material. At pressures of 500 Pa with the reduced flow rate the deposit was not analogous of those found in irradiated material, suggesting that the most representative deposit is formed at system pressure of 1000 Pa with a 50 cm³ min^{−1} flow of 10% CH₄:90% Ar.

Growth using ¹³C precursor gas showed a similar topography/morphology to ¹²C deposits indicating that there is no appreciable difference in the growth mechanism between the different isotopes, thereby justifying the use of this simulant to study the behaviour of carbonaceous deposits found on irradiated graphite. The clear separation of the deposit and underlying graphite shown by isotopic imaging using a MS-SIMS has shown that a deposit is formed, and cross-sectional images indicate that the topography and morphology are very similar to the ones found on irradiated graphite. Catalyst stage Raman spectroscopy combined with TGA have shown these deposits to be of a similar reactivity to those found on irradiated graphite. These deposits appear to be suitable for further studies involving microbial systems to examine the possible release of the deposit into the environment in a geological disposal facility. Based on the thermal oxidation behaviour, the density difference in the surface deposit materials between irradiated and simulant samples does not appear to significantly influence observed reactivity. With the surface layers exhibiting rapid degradation at much lower temperatures than the underlying graphite.

5. Conclusion

Carbonaceous ¹²C and ¹³C deposits were formed on Pile Grade A graphite using microwave plasma deposition and examined using Focused Ion Beam, Scanning Electron Microscopy and Magnetic Sector-Secondary Ion Mass Spectrometry. Several conclusions can be drawn:

1. The surface topography of both ¹²C and ¹³C deposits formed by MPCVD are very similar to the 'cauliflower-like' deposits found on graphite samples trepanned from a Magnox reactor.
2. Deposits formed at 1000 Pa system pressure with a 50 cm³ min^{−1} flow of 10% CH₄:90% Ar showed the closest resemblance to the deposits on the irradiated material.
3. The internal morphology of the deposit is slightly more porous than that found in irradiated graphite. However, variations in methane concentrations and gas pressure can affect the density of deposited material.

To summarise, there is a potential use of the ¹³C containing deposits synthesised in this work to act as simulants in future studies aimed at better understanding and predicting the post-disposal behaviour of irradiated graphite waste in a geological disposal environment and the associated release profile of ¹⁴C

arising from the labile deposit.

Acknowledgements

The authors would like to thank the EPSRC and Radioactive Waste Management for the funding of this work (The post-disposal Behaviour of C-14 and Irradiated Graphite [BIG], Grant No EP/1036354/1). The support of our co-workers at the University of Huddersfield (www.hud.ac.uk/c-14-big) and advice from colleagues in Magnox Ltd and the National Nuclear Laboratory is also gratefully acknowledged. All relevant data are available on Harvard Dataverse at DOI: <http://dx.doi.org/10.7910/DVN/5GZ4JK>.

References

- [1] Nuclear Decommissioning Authority, Higher Activity Waste, The Long-term Management of Reactor Core Graphite Waste Credible Options (Gate A), 2013. SMS/TS/D1-HAW-6/002/A.
- [2] Nuclear Decommissioning Authority, Geological Disposal, Carbon-14 Project – Phase 1 Report, 2012. NDA/RWMD/092.
- [3] P.J. Heard, L. Payne, M.R. Wootton, P.E.J. Flewitt, Evaluation of surface deposits on the channel wall of trepanned reactor core graphite samples, *J. Nucl. Mater.* 445 (1–3) (2014) 91–97.
- [4] L. Payne, P.J. Heard, T.B. Scott, in: Enrichment of C-14 on Surface Deposits of Oldbury Reactor Graphite Investigated with the Use of Magnetic Sector Secondary Ion Mass Spectrometry Waste Management Symposia 2015 Proceedings, 2015.
- [5] X. Hou, Rapid analysis of ¹⁴C and ³H in graphite and concrete for decommissioning of nuclear reactor, *Appl. Radiat. Isotopes* 62 (6) (2005) 871–882.
- [6] G. Baston, T. Marshall, R. Otlet, A. Walker, I. Mather, S. Williams, Rate and speciation of volatile carbon-14 and tritium releases from irradiated graphite, *Mineral. Mag.* 76 (8) (2012) 3293–3302.
- [7] A. Malesevic, S. Vizireanu, R. Kempes, A. Vanhulsel, C.V. Haesendonck, G. Dinescu, Combined growth of carbon nanotubes and carbon nanowalls by plasma-enhanced chemical vapor deposition, *Carbon* 45 (15) (2007) 2932–2937.
- [8] K. Bystrov, J. Westerhout, M. Matveeva, A. Litnovsky, L. Marot, E. Zoethout, et al., Erosion yields of carbon under various plasma conditions in Pilot-PSI, *J. Nucl. Mater.* 415 (1) (2011). S149–S52.
- [9] S.G. Wang, Q. Zhang, S.F. Yoon, J. Ahn, D.J. Yang, Q. Wang, et al., Electron field emission from carbon nanotubes and undoped nano-diamond, *Diam. Relat. Mater.* 12 (1) (2003) 8–14.
- [10] M.L. McConnell, D.P. Dowling, C. Pope, K. Donnelly, A.G. Ryder, G.M. O'Connor, High pressure diamond and diamond-like carbon deposition using a microwave CAP reactor, *Diam. Relat. Mater.* 11 (3–6) (2002) 1036–1040.
- [11] M. Castro, R. Cuerno, M. Nicoli, L. Vázquez, J.G. Buijnsters, Universality of cauliflower-like fronts: from nanoscale thin films to macroscopic plants, *New J. Phys.* 14 (10) (2012) 103039.
- [12] A.J. Wickham, R.M. Sellers, N.J. Pilkington, Graphite Core Stability During “Care and Maintenance” and “Safe Storage”, 1998. Vienna, IAEA-TECDOC 1043.
- [13] A.J. Wickham, L. Rahmani, Graphite Dust Explosibility in Decommissioning: a Demonstration of Minimal Risk, 2010. Vienna, IAEA-TECDOC-1647.
- [14] R. Burcl, Characterization, Treatment and Conditioning of Radioactive Graphite from Decommissioning of Nuclear Reactors, 2006. Vienna, Austria, IAEA-TECDOC-1521.
- [15] P. Minshall, I. Sadler, A. Wickham, Radiolytic graphite oxidation revisited, in: Poster Presented at Specialists Meeting on Graphite Moderator Lifecycle Behaviour, IAEA, Bath (United Kingdom), 1996.
- [16] R. Moskovic, P.J. Heard, P.E.J. Flewitt, M.R. Wootton, Overview of strength, crack propagation and fracture of nuclear reactor moderator graphite, *Nucl. Eng. Des.* 263 (0) (2013) 431–442.
- [17] P.W. May, Diamond thin films: a 21st-century material, *Philos. Trans. R. Soc. Lond. Ser. A Math. Phys. Eng. Sci.* 358 (1766) (2000) 473–495.
- [18] S.E. Harton, F.A. Stevie, H. Ade, Carbon-13 labeling for improved tracer depth profiling of organic materials using secondary ion mass spectrometry, *J. Am. Soc. Mass Spectrom.* 17 (8) (2006) 1142–1145.
- [19] G. Silbermann, N. Moncoffre, N. Toulhoat, N. Béreder, A. Perrat-Mabilon, G. Laurent, et al., Temperature effects on the behavior of carbon 14 in nuclear graphite, *Nucl. Instrum. Methods Phys. Res. Sect. B Beam Interact. Mater. Atoms* 332 (0) (2014) 106–110.
- [20] Lancashire UoC. Contaminated material patent GB1312312.0. 2013 9th July 2013.
- [21] P.J. Heard, K.A. Feeney, G.C. Allen, P.R. Shewry, Determination of the elemental composition of mature wheat grain using a modified secondary ion mass spectrometer (SIMS), *Plant J.* 30 (2) (2002) 237–245.
- [22] P.J. Heard, M.R. Wootton, R. Moskovic, P.E.J. Flewitt, Crack initiation and propagation in pile grade A (PGA) reactor core graphite under a range of loading conditions, *J. Nucl. Mater.* 401 (1–3) (2010) 71–77.
- [23] J.S. Lee, I. Gilmore, M. Seah, I. Fletcher, Topography and field effects in secondary ion mass spectrometry – part I: conducting samples, *J. Am. Soc. Mass*

- Spectrom. 22 (10) (2011) 1718–1728.
- [24] N.T. Kita, T. Ushikubo, B. Fu, J.W. Valley, High precision SIMS oxygen isotope analysis and the effect of sample topography, *Chem. Geol.* 264 (1) (2009) 43–57.
- [25] S. Rangarajan, B.J. Tyler, Topography in secondary ion mass spectroscopy images, *J. Vac. Sci. Technol. A* 24 (5) (2006) 1730–1736.
- [26] S. Rajsiri, B. Kempshall, S. Schwarz, L. Giannuzzi, FIB Damage in Silicon: amorphization or Redeposition? *Microsc. Microanal.* 8 (S02) (2002) 50–51.
- [27] C14-BIG. 2014 [cited; Available from: <http://www.hud.ac.uk/c14-big/>].
- [28] C. Bower, O. Zhou, W. Zhu, D.J. Werder, S. Jin, Nucleation and growth of carbon nanotubes by microwave plasma chemical vapor deposition, *Appl. Phys. Lett.* 77 (17) (2000) 2767–2769.
- [29] L.C. Qin, D. Zhou, A.R. Krauss, D.M. Gruen, Growing carbon nanotubes by microwave plasma-enhanced chemical vapor deposition, *Appl. Phys. Lett.* 72 (26) (1998) 3437–3439.
- [30] K. Kobashi, K. Nishimura, Y. Kawate, T. Horiuchi, Synthesis of diamonds by use of microwave plasma chemical-vapor deposition: morphology and growth of diamond films, *Phys. Rev. B* 38 (6) (1988) 4067–4084.
- [31] B.R. Stoner, J.T. Glass, Textured diamond growth on (100) β -SiC via microwave plasma chemical vapor deposition, *Appl. Phys. Lett.* 60 (6) (1992) 698–700.
- [32] C-s Yan, Y.K. Vohra, H-k Mao, R.J. Hemley, Very high growth rate chemical vapor deposition of single-crystal diamond, *Proc. Natl. Acad. Sci.* 99 (20) (2002) 12523–12525.
- [33] S.E. Jensen, E. Nonbol, Description of the Magnox Type of Gas Cooled Reactor (MAGNOX), 1999. NKS/RAK-2(97)TR-C5.